Journal of Materials Chemistry A

Layered Electrides as Fluoride Intercalation Anodes

Journal:	*Journal of Materials Chemistry A*
Manuscript ID	TA-ART-06-2020-006162.R1
Article Type:	Paper
Date Submitted by the Author:	21-Sep-2020
Complete List of Authors:	Hartman, Steven; Washington University in Saint Louis, Institute of Materials Science and Engineering Mishra, Rohan; Washington University in Saint Louis, Mechanical Engineering and Materials Science; Washington University in Saint Louis, Institute of Materials Science and Engineering

Layered Electrides as Fluoride Intercalation Anodes

Steven T. Hartman,[†,⊥] and Rohan Mishra[‡,†,]*

[†]Institute of Materials Science and Engineering, Washington University in St. Louis, One Brookings Drive, St. Louis, MO 63130, USA

[‡]Department of Mechanical Engineering and Materials Science, Washington University in St. Louis, One Brookings Drive, St. Louis, MO 63130, USA

*Email: S.T.H. (steven.t.hartman@wustl.edu) or R.M.(mailto:rmishra@wustl.edu)

ABSTRACT: The fluoride ion is well suited to be the active species of rechargeable batteries, due to its small size, light weight, and high electronegativity. While existing F-ion batteries based on conversion chemistry suffer from rapid electrode degradation with cycling, those based on fluoride intercalation are currently less attractive then cation intercalation battery chemistries due to their low reversible energy densities. Here, using first-principles density-functional-theory calculations, we predict that layered electrides, such as Ca_2N and Y_2C — that have an electron occupying a lattice site — are promising hosts for fluoride intercalation, since their anionic electrons create large interstices. Our calculations indicate that anodes made from layered electrides can offer voltage up to –2.86 V vs. La_2CoO_4 cathode, capacity >250 mAh/g, and fast diffusion kinetics with migration barriers as low as 0.15 eV. These metrics compare favorably to popular Li-ion intercalation cathodes such as $LiCoO_2$. Electrides open up a new space for designing fluorine intercalation batteries with good performance and cyclability.

TOC GRAPHIC

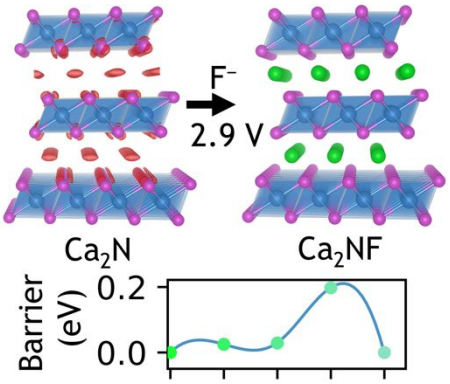

Rechargeable batteries enable crucial modern technologies, such as mobile phones, electric cars, and aerial drones, and will be required in even larger numbers for the rapidly growing automotive fleets and grid-scale storage of electricity generated by intermittent renewable sources. Currently, the market is dominated by Li-ion batteries, which shuttle lithium ions between two intercalation electrodes such as graphite and $LiCoO_2$. In these electrodes, the Li ions move into empty spaces in a host material without significantly disrupting the host's structure. While this design has achieved high energy density and adequate cycling stability, the supply risk of lithium and cobalt[1] is predicted to create obstacles for the surge in battery usage. Current Li-ion batteries also pose safety concerns due to Li dendrite growth and thermal runaway.[2] Therefore, it is desirable to find other high-performance battery chemistries besides Li-ion.

The search for alternative chemistries has primarily been limited to light cations such as Na^+,[3] K^+,[4] Mg^{2+},[5] Zn^{2+},[6] and Al^{3+}.[7] A handful of studies have instead focused on using anions as the active species.[8, 9] Amongst the various candidates for active anion batteries, fluoride (F^-) is especially attractive due to its earth-abundance, light weight, high electronegativity, and reasonably fast diffusion in liquid or solid electrolytes.[10-17] In contrast to the success of Li batteries using two intercalation electrodes, most research on fluoride-ion batteries (FiBs) has followed a different path involving conversion reactions,[18, 19] pairing metals with metal fluorides, such as:[11]

$$3Sn + 2BiF_3 \rightarrow 3SnF_2 + 2Bi.$$

The theoretical current capacity of conversion electrodes can be very high, such as 669 mAh/g for Ca/CaF_2, compared to 294 mAh/g for $LiCoO_2$. However, these high capacities are difficult to achieve in practice. The phase transformation of the metal to its fluoride during charge/discharge cycles is typically a slow reaction which requires a large overpotential; furthermore, if the resulting volume change is large, the electrode can crumble and degrade during repeated cycling.[20] In addition, the pure metal electrode sometimes dissolves into the electrolyte, further degrading it.[19] These effects are also seen in Li-ion conversion batteries, which have not found commercial success despite extensive research.[21] Therefore, prior experience suggests the value of intercalation FiBs, but high-capacity, fluoride intercalation electrodes

have been not been reported. The first F^- intercalation electrode to be tested was $LaSrMnO_4/LaSrMnO_4F_2$,[13] which offered a moderate theoretical capacity of 172 mAh/g, but proved to have very limited reversibility due to destructive side reactions and overpotentials >1 V. La_2CoO_4/La_2CoO_4F later provided improved cycling durability, but at the cost of low theoretical capacity (67 mAh/g).[18, 22] These electrodes have relatively little driving force for fluoride intercalation, making them suitable for cathodes, while FiB intercalation anodes have not yet been demonstrated.

In this Article, we take a new approach to design intercalation FiBs, which is to use the unconventional chemistry of electride crystals to our advantage. These inorganic electrides have interstices occupied by free electrons that act as anions, due to their unusual stoichiometries, which are not charge-balanced in common oxidation states.[23] We use first-principles density-functional-theory (DFT) calculations to show that electrides can intercalate fluoride stably by replacing the free electron with a F^-. Among the 12 known or predicted electrides which we have examined, we predict Ca_2N and Y_2C as promising candidates for intercalation anodes with theoretical gravimetric capacities ~280 mAh/g, volume change during cycling <15%, voltage <–2.5 V vs. La_2CoO_4 cathode, and low kinetic barriers <0.2 eV for fluoride ion transport. These values approach the performance of popular Li-ion electrodes such as $LiCoO_2$, which has a theoretical capacity 295 mAh/g, calculated voltage 3.7 V vs. graphite, and migration barriers ~0.3 eV,[24] and Ca_2N in particular is much more earth-abundant than $LiCoO_2$. The excellent performance metrics of Ca_2N and Y_2C, if realized experimentally, will be a major step toward the practical use of FiBs.

First, we consider the crystal structures of Li-intercalation electrodes, to see if the proven design principles can be transferred directly to FiBs. Two of the most successful Li^+ intercalation cathodes, $LiFePO_4$[25] and $LiCoO_2$,[26] are shown in Figures 1a and b, respectively. They are characterized by anionic polyhedra that are centered on small, highly charged cations (Shannon radius of 0.65 Å for Fe^{3+}, 0.17 Å for P^{5+}, and 0.53 Å for Co^{4+}). The Li^+ ions rest in the interstices between these polyhedra. The transition metal ions, besides providing the redox activity by changing their oxidation state, also serve to hold the crystal together when the Li^+ is absent (in the charged state). Thanks to these framework-preserving cations,

$LiCoO_2$ and $LiFePO_4$ have calculated volume changes of only 3% and 7 %,[24] respectively, as Li is removed, promoting durability over many cycles.

Based on these examples, to intercalate F^-, we ought to invert the paradigm and have cationic polyhedra centered on some other anion, to maintain the structural integrity in the absence of F^- ions. However, we immediately notice that anions are generally larger than cations,[27] with F^- having the smallest Shannon radius of 1.33 Å. In addition to making fluoride intercalation more challenging, the large size of anions also restricts the construction of anion-centered polyhedra. Therefore, the best candidates for anion-centered polyhedra are the first-row species N^{3-}(1.46 Å), B^{3-}, C^{4-}, and possibly O^{2-} (1.4 Å).[28, 29] As for the surrounding cations, they should be large enough to create stable polyhedra with spacious interstices between them. They should also have a low charge to achieve charge balance, since they are more numerous than the central anion even if the polyhedra share many edges and faces. The cation also needs to be light for good gravimetric capacity, and inexpensive. Finally, it ought to be redox-active, with several stable oxidation states.

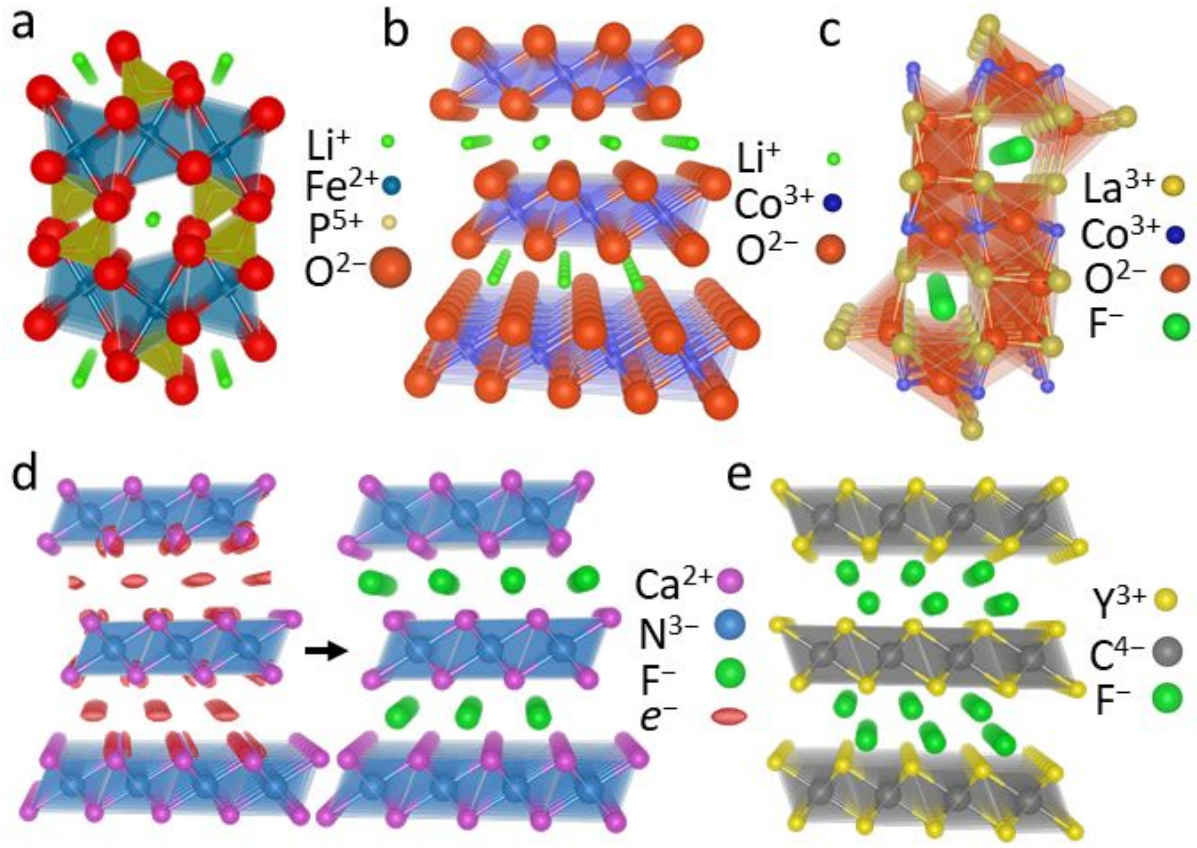

Figure 1. **Structural principles for fluorine intercalation electrode design**. **a.** The popular Li-ion intercalation electrode $LiFePO_4$, in which Li^+ (green) occupies distorted octahedral sites between PO_4 tetrahedra and FeO_6 distorted octahedra. **b.** $LiCoO_2$, with Li^+ sitting in octahedral interstices between layers of edge-sharing CoO_6 octahedra. **c**. The previously known F^- intercalation electrode La_2CoO_4F, with F^- (green) in tetrahedral interstices between strongly distorted La_5CoO octahedra. **d.** The newly proposed Ca_2NF electrode, with F^- in octahedral interstices between layers of edge-sharing Ca_6N octahedra. The localized electrons between the Ca_2N layers are shown with isosurfaces of the electron localization function. Ca_2NF's structure is the inverse of $LiCoO_2$'s structure in **b**. **e.** Y_2CF_2, with F^- in tetrahedral interstices between layers of edge-sharing Y_6C octahedra.

These constraints are not easily satisfied by a single cation, and indeed all existing fluoride intercalation electrodes combine two or more cation species. Figure 1c shows the most successful electrode to date, La_2CoO_4F,[18, 22] which uses the larger La^{3+} cations (1.16 Å) to create large tetrahedral sites for F^- in the rock-salt structured LaO layers. The smaller Co^{2+} (0.65 Å) occupies CoO_2 layers which provide the redox activity, as F^- intercalation onto the LaO layers oxidizes Co to 3+. However, the gravimetric capacity is low (67 mAh/g theoretically) because the heavy La is "dead weight" from an electrochemical perspective. This is

generally true for similar electrodes such as $MgFeSb_4O_8F$ (39 mAh/g)[30] or $FeSb_2O_4F$ (74 mAh/g) [31]although it can be mitigated by using cations lighter than La or Sb, such as Sr (1.26 Å) in $Sr_2TiO_3F_2$ (197 mAh/g), which has been proposed as a FiB anode but not yet tested.[32]

We conclude that to keep the electrode light, yet retain large interstitial sites, it should ideally have only one type of cation. Alkali and alkaline earth metals are light, large, inexpensive, and have low charge, satisfying all the constraints except redox activity, so we can expect good results if these metals can be stabilized in oxidation states besides +1 and +2, respectively. Such materials are rare, but a small group of suboxides, subnitrides, and hypocarbides are stable with fewer anions than would be expected by charge balance.[33] One well-studied example is the electride Ca_2N, which from a chemical perspective can be represented as $Ca_2^{2+}N^{3-}e^-$, where e^- is an electron localized at an empty anion site. We show the structure of Ca_2N in Figure 1d. Ca_2N has an inverse $LiCoO_2$ structure, with Ca_6N octahedra instead of CoO_6, and Li replaced by anionic electrons. This suggests the following half-reaction can proceed topochemically, with little volume change:

$$Ca_2N + F^- \rightarrow Ca_2NF + e^- \quad [1]$$

While Ca_2N is referenced as a possible FiB electrode in a patent application,[34] any related studies remain unpublished beyond a single voltammogram, so a detailed theoretical study offers the first opportunity to understand the F^- intercalation properties of Ca_2N.

To assess the intercalation of Ca_2N with F^- ions, we have calculated the stability of the products and reactants for a variety of fluoride intercalation reactions along with the associated change in voltage and volume using DFT. For details of these calculations, see the section on Computational Methods. We find that both Ca_2N and Ca_2NF, with their structures shown in Figure 1d, are on the convex hull, and hence, stable against decomposition into known competing phases present in the Materials Project database.[24] The fluoride ion occupies the octahedral site between Ca_2N layers, while the tetrahedral sites, which are twice as many as the octahedral sites, are unoccupied. Placing fluoride into the tetrahedral site costs 0.34 eV more than the octahedral site. Upon geometry optimization, we find that Ca_2NF retains the same rhombohedral *R*

$\bar{3}m$ phase as Ca_2N. For this structure, we can calculate its gravimetric capacity to be 285 mAh per gram of Ca_2N according to Eqn. 1:

$$\frac{1\text{ mol } Ca_2N}{94\text{ g } Ca_2N}\times\frac{1\text{ mol } e^-}{1\text{ mol } Ca_2N}\times\frac{96485\text{ A}\times\text{s}}{1\text{ mol } e^-}\times\frac{1000\text{ mA}}{1\text{ A}}\times\frac{1\text{ h}}{3600\text{ s}}=\frac{285\text{ mAh}}{1\text{ g}} \quad [2]$$

We note that while Ca_2NCl and Ca_2NBr are experimentally reported to exist in the $R\bar{3}m$ phase,[35, 36] Ca_2NF has only been made in the $I4_1/amd$ phase,[37] which we find is 5 meV/atom higher in energy than the $R\bar{3}m$ phase. Therefore, we expect that low-temperature fluoridation, which has emerged as a successful strategy to produce fluoride structures topochemically,[38, 39] should yield $R\bar{3}m$ Ca_2NF from $R\bar{3}m$ Ca_2N. Space groups $I4_1/amd$ and $R\bar{3}m$ do not have a group-subgroup relationship, so any transformation from one to the other would be a reconstructive transition,[40] requiring many chemical bonds to break and re-form. Once Ca_2NF is kinetically trapped in the layered structure, the strength of the metal-nitride bonds will hinder the formation of other competing phases during cycling. We note that the isostructural $LiCoO_2/CoO_2$ electrode is metastable with respect to non-layered phases at both ends of the phase diagram,[24] using the same computational methods we use here. CoO_2's layered phase is metastable by 6 meV/atom relative to an $I4/m$ phase, while $LiCoO_2$ has an $Fd\bar{3}m$ phase which is 193 meV/atom more stable, but careful management of the cycling can preserve the useful layered phase. The $R\bar{3}m$ phase of Ca_2NF shrinks 13% by volume during fluoridation, and the electromotive force is –2.86 V vs. La_2CoO_4/La_2CoO_4F, calculated with:

$$\frac{E_{Ca_2NF}+E_{La_2CoO_4}-E_{Ca_2N}-E_{La_2CoO_4F}}{1}=-2.86\text{ V}, \quad [3]$$

where E_{Ca_2NF} and $E_{La_2CoO_4}$ are the calculated energies of the products, E_{Ca_2N} and $E_{La_2CoO_4F}$ are the energies of the reactants, and 1 is the number of electrons transferred in the reaction. –2.86 V is the same calculated potential as the Li/LiF half-reaction, indicating that Ca_2N is highly electropositive, consistent with its experimentally known sensitivity to air and moisture.[41] Charge-balanced Ca_2NF can be further fluoridated to Ca_2NF_2 at –0.78 V vs. La_2CoO_4/La_2CoO_4F, which corresponds to an oxidation of nitride to the unstable N^{2-}. We do not include this in Ca_2N's theoretical capacity, since it is not clear if the anion-redox capacity is accessible without degrading the electrode. The Ca_2NF_2 phase is 237 meV/atom above the Materials

Project convex hull, excluding species such as CaN_6 which are poorly described by DFT,[42] and it might decompose by nitrogen gas evolution to produce Ca_2NF and CaF_2. Therefore, it is likely necessary to cut off the reaction after the first fluoridation, such as by using a small excess of anode material.

Another electride isostructural to Ca_2N, Y_2C,[43] is also a promising candidate for FiB anodes. Y_2C, as shown in Figure 1e, can be represented as $Y_2^{3+}N^{3-}2e^-$ with $2e^-$ nominally residing at the octahedral sites. Recently, Druffel et al. reported the formation of Y_2CF_2 using a high-temperature solid-state reaction of Y, YF_3, and graphite.[44] F^- ions are observed to occupy the tetrahedral sites between the Y_2C layers of Y_2CF_2, and the Y_2C layers re-stack from their original *ABC* stacking pattern to an *AAA* stacking in Y_2CF_2 with space group $P\bar{3}m1$, as shown in Figure 1e. The *AAA* stacking of Y_2C is only 28 meV/atom less stable than *ABC*, so it may appear as a metastable phase during charge/discharge cycles. The structural restacking may also create a significant interfacial strain between the fluoridated and unfluoridated phases, which is an important matter for further investigation. We find that Y_2CF_2 expands by 9% in volume relative to Y_2C, in good agreement with the 8% volume difference found experimentally. We also calculate the fluoridation voltage to be –2.56 V vs. La_2CoO_4/La_2CoO_4F, and a gravimetric capacity of 282 mAh/g.

The intermediate Y_2CF phase, with F^- in octahedral sites, is unstable by 81 meV/atom with respect to Y_2C and Y_2CF_2, indicating that Y_2C is likely to fluoridate in a one-step process without staging. Further evidence for a one-step reaction is provided by the formation energy of the neutral F^- vacancy, which we calculate to be 0.14 eV at the chemical potential defined by the Y_2C/Y_2CF_2 equilibrium. Creating two adjacent fluoride vacancies costs 0.46 eV. Neglecting entropy, it is easier to defluoridate Y_2CF_2 all at once, than to remove one or two F^- at a time. Most Li-ion batteries discharge in stages because the electrostatic repulsion between Li^+ gradually reduces the driving force to insert additional Li^+,[45] but the empty octahedral F^- sites of the electrides can still be occupied by a negatively charged electron, so an electrostatic repulsion still occurs in the empty state. We have calculated the electrostatic interactions using VESTA,[46] assuming that all anionic free electrons are localized in the octahedral interstitial site. Y_2CF_2 has a total Madelung energy of –174 eV/f.u., compared to –185 eV/f.u. for Y_2C. This includes the contribution of the re-stacking;

Ca_2NF does not re-stack, and has a Madelung energy of –89.5 eV/f.u., much closer to the –87.8 eV/f.u. of Ca_2N. As a comparison, the Madelung energy of $LiCoO_2$ is –110 eV/f.u. and that of CoO_2 is –140 eV/f.u..

Based on these thermodynamic calculations, we expect the layered electrides to have good energy storage capacity, but the diffusion kinetics are also important. To achieve high power density, a battery electrode must conduct the active ion rapidly. Since the layered structures of Ca_2NF and Y_2CF_2 match $LiCoO_2$ so closely, it is reasonable to expect them to have fast two-dimensional ion transport kinetics, which we calculate using the climbing-image nudged elastic-band (NEB) technique.[47] To provide a benchmark, we first calculate the vacancy diffusion mechanism of the known cathode material La_2CoO_4F, which is shown in Figure 2a, with a barrier to fluoride migration of 0.83 eV. For the layered electrides, we consider three mechanisms: vacancy-assisted diffusion, direct interstitial diffusion, and interstitialcy (kick-out) diffusion. The lowest barrier for Ca_2NF is the interstitialcy diffusion mechanism, in which a tetrahedral interstitial F^- displaces an octahedrally coordinated F^-, forcing it into an adjacent tetrahedral interstitial site. The high-energy transition state, with a saddle point barrier height of only 0.2 eV, is associated with a configuration where the two diffusing F^- ions pass through triangular openings in the Ca^{2+} sublattice. Y_2CF_2 is more likely to exhibit vacancy diffusion, with a barrier of 0.16 eV as the F^- passes directly between the two Y^{3+} that are shared between the starting and ending tetrahedral sites. Both of these barriers compare favorably to the calculated barrier of 0.2-0.3 eV for Li^+ diffusion in $LiCoO_2$.[48]

The NEB barriers assume the existence of an empty defect site (interstitial for Ca_2NF and F-vacancy for Y_2CF_2), but the total activation energy E_A for diffusion is the formation energy of the relevant electrically neutral defect, plus the kinetic barrier height. When calculating the formation energy of the defects, we can assume either fluorine-rich and fluorine-poor conditions, which are the fluoride chemical potentials required to defluoridate or further fluoridate the electride. In Ca_2NF, the dominant mechanism switches from interstitialcy to vacancy diffusion when the

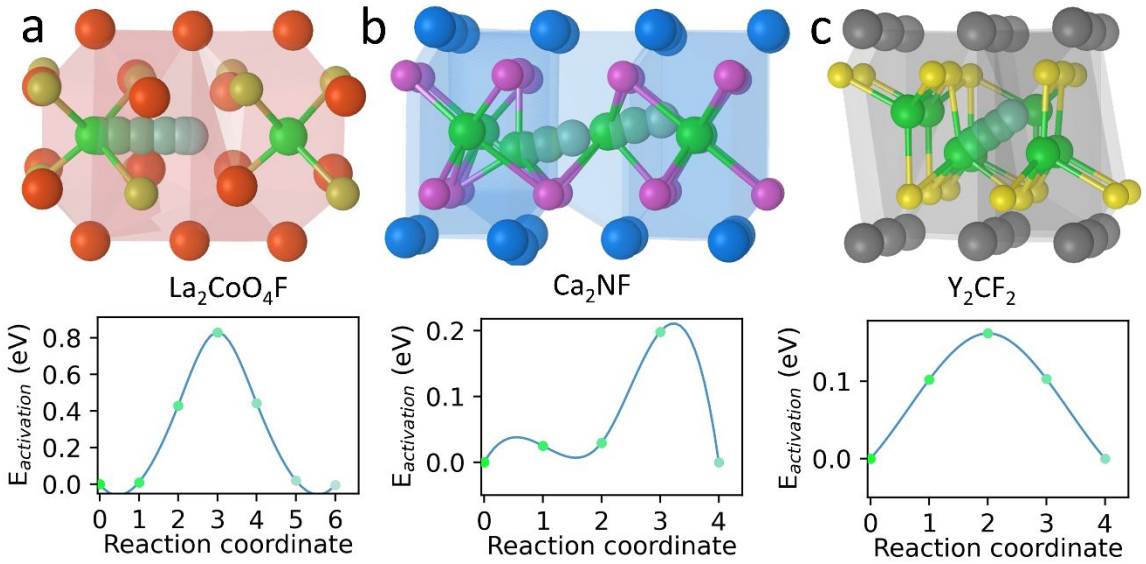

Figure 2: NEB study of F^- diffusion kinetics. a. Vacancy diffusion in La_2CoO_4F. A tetrahedral F^- moves to an adjacent vacant tetrahedral site in the LaO layer. The plot shows the diffusion barrier for the motion of F^-. **b.** Interstitialcy mechanism in Ca_2NF. A tetrahedral F^- interstitial displaces an octahedral F^-, which moves to a tetrahedral interstitial site on the opposite side as the original. **c.** Vacancy diffusion mechanism in Y_2CF_2. A tetrahedral F^- moves to an adjacent tetrahedral site.

fluoride chemical potential is reduced, because the fluoride interstitial costs 2.3 eV to form under fluoride-poor conditions while the F^- vacancy only costs 0.3 eV. The vacancy diffusion has a barrier of 1.34 eV which occurs as the moving F^- passes through the tetrahedral site. In contrast, we predict that Y_2CF_2 favors vacancy diffusion under any stable fluoride potential, since the F^- vacancy's formation energy never exceeds 0.6 eV. The total calculated activation energies are 1.61-1.64 eV for Ca_2NF and 0.30-0.71 eV for Y_2CF_2, indicating that Y_2CF_2 is likely to have much faster kinetics. We estimate the diffusivity D using Eqn. 3:[48]

$$D = \frac{l^2 v_0}{2n} \exp\left(-\frac{E_A}{kT}\right) \quad [4]$$

Here the dimensionality $n = 2$, l is the length of a single jump, and k is the Boltzmann constant. We approximate the attempt frequency, $v_0 = 10^{13}$/s, a fairly typical value for fluorides; for example, the attempt frequency of BaF_2 was estimated to be 0.6 x 10^{13}/s from the frequency of the transverse optical phonon

mode.[49, 50] We obtain a negligible value of $D = 2.4 \times 10^{-30}$ cm^2/s for Ca_2NF at 298 K and F-poor conditions, while Y_2CF_2 has $D = 1.4 \times 10^{-8}$ cm^2/s.

We have also used ab-initio molecular dynamics (AIMD) calculations as an alternate method to calculate the intrinsic activation energy and diffusivity of stoichiometric Y_2CF_2 without artificially imposed defects. We run the calculations at elevated temperatures to obtain a meaningful number of diffusion events in a computationally affordable timescale. By running for 35 ps at 1700 K, 1800 K, 1900 K, 2000 K, and 2100 K, we obtain the mean-squared displacement (MSD) over time, and the diffusivity, at each temperature. Fitting the temperature-dependent diffusivities to an Arrhenius relationship provides the total activation energy.[51, 52] We find that the total activation energy of F^- diffusion in Y_2CF_2 is 0.75 eV ± 0.25, which yields a diffusivity at 300 K of 6.9×10^{-16} cm^2/s. These values agree well with the NEB-calculated values for the fluoride-rich condition, where F vacancies have higher formation energy and are present only at lower concentrations. In the AIMD simulations, we observe both the vacancy and interstitialcy diffusion mechanisms. However, the AIMD supercells are stoichiometric, so the defects must be generated as interstitial/vacancy pairs. For this reason, many of the hopping events we observe either create or annihilate defects, as opposed to the defect-conserving mechanisms we calculate with NEB.

Experimentally, sample characteristics such as grain size will also influence the experimental diffusivity.[53] Since the majority of the total activation energy is the vacancy formation cost, doping Y_2CF_2 with a small amount of Ca^{2+} ought to improve the diffusion kinetics by introducing additional F^- vacancies to compensate charge. Likewise, Ca_2NF's interstitialcy diffusion has a low kinetic barrier height <0.2 eV, so we expect the diffusion can be enhanced by doping with Y^{3+} to increase F^- interstitial concentration.

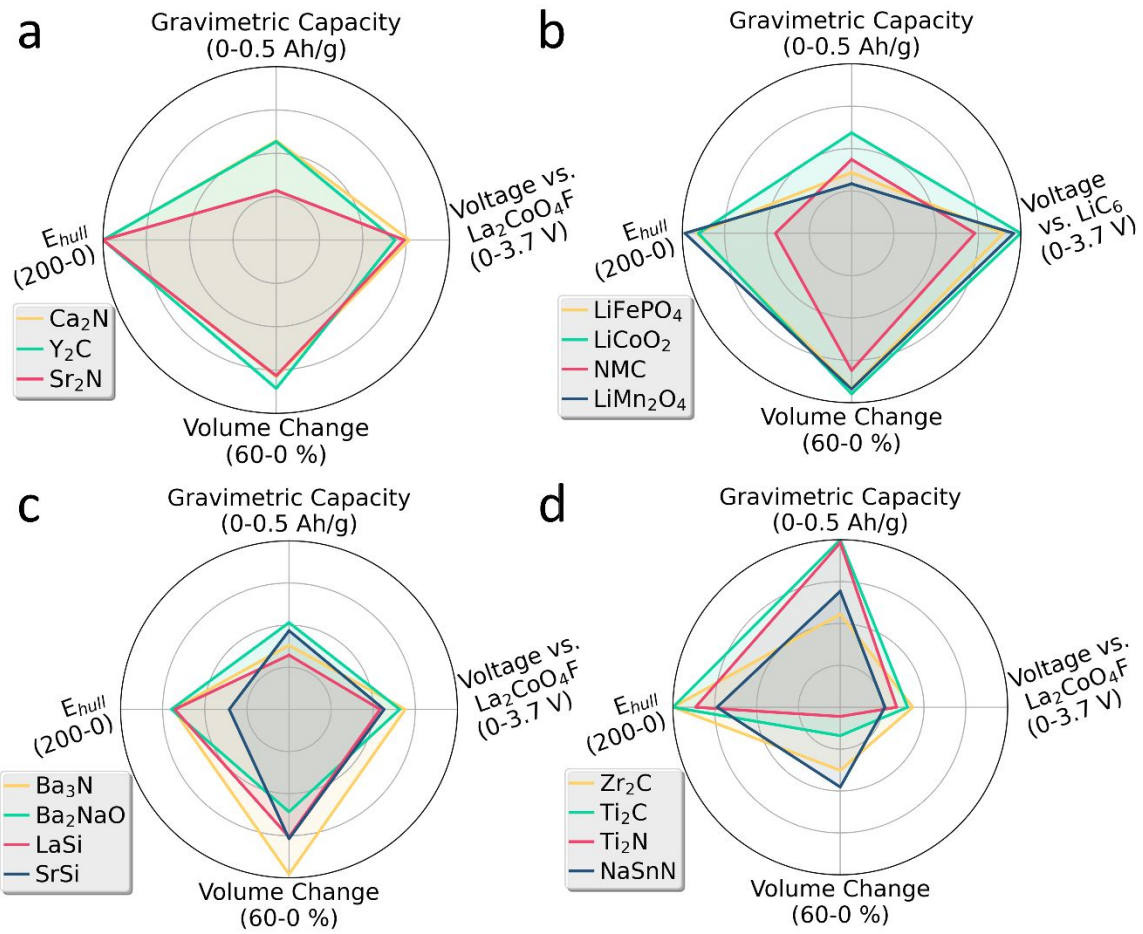

Figure 3: **Comparison of structural families for intercalation electrodes.** Gravimetric capacity and voltage are normalized with respect to the highest score in each category. The voltage is the average voltage for the complete reaction with La_2CoO_4F or LiC_6, not accounting for any steps in the voltage profile. Thermodynamic stability is measured with the hull energy $E_{hull,}$ in meV/atom, of whichever electrode state (charged or discharged) is less stable, and plotted from 200 meV above the hull to 0. Likewise, the magnitude of the volume change of the intercalated phase with respect to the de-intercalated phase is plotted from 60% to 0%. Calculated data for these and other electrodes are in Supporting Information. **a.** The layered electrides which are the focus of this work. **b.** Commercially successful Li-ion battery cathodes, for comparison. **c.** Other predicted electrides with different structures than Ca_2N. **d.** 2D mxenes, and the closely related material NaSnN.

While Ca_2N and Y_2C are the most promising electrides for use in FIBs identified in this study, we have also calculated the F^- intercalation properties of several other electrides, including LaSi, SrSi, Ba_3N, and Ba_2NaO,[54-56] for comparison. In addition, we have calculated the stability and capacity of several known MXenes,[29] which are structurally related to the layered electrides, although their chemical properties are

different. We compare the theoretical performance of these different structural families in Figure 3, with popular Li-ion electrodes shown as a reference. Ca_2N and Y_2C have calculated performances closest to that of their structural analogue $LiCoO_2$, with excellent thermodynamic stability and current capacity. The other electrides are not as promising, since their structures do not allow fluoride intercalation with the same stability as the layered electrides. However, the structure alone is not enough without the electride chemistry. The isostructural MXenes have high gravimetric capacity — up to 497 mAh/g for Ti_2C — due to their light weight, but also have low voltage and experience large volume changes. The electride chemistry turns out to be essential because the free anionic electrons have a very low work function ~2.5 eV,[57] the same as Li metal.[58] Because electrides give up electrons easily, they have a higher voltage vs. the cathode. The anionic electrons also improve the cycling stability by acting in combination with the large Ca^{2+} and Y^{3+} cations to maintain large interstices even in the unfluoridated state.

Our calculations suggest that Ca_2N and Y_2C can perform very well as FiB anodes. Going forward, there are several other FiB components which require improvement for these anodes to be used at their full capability. The most important target for further research is the voltage stability window of the electrolyte and the conductive additive. Ca_2N is likely to form a solid-electrolyte interphase (SEI) in contact with solid fluoride electrodes such as $La_{1-x}Ba_xF_{3-x}$ (LBF), since Li/LiF has the same potential of –2.86 V and is known to reduce LBF,[59] while Y_2C is right on the edge of the stability window. The effect of this SEI is not yet known, and it might be preferable to find an electrolyte which is stable against Ca_2N. At the other end of the voltage window, La_2CoO_4 is the highest-voltage practical cathode, at 2.86 V vs. Ca_2N/Ca_2NF. Higher-voltage cathodes are known, such as $MgFeSb_4O_4$ (3.37 V)[30] or $FeSb_2O_4$ (3.49 V)[31] but at those voltages the commonly used conductive additive, carbon black, reacts irreversibly with F^-.[13, 30, 59] The carbon fluoridation may be avoided in the future through the introduction of improved conductors such as SnO_2 or carbon nanotubes;[20] success in this endeavor would increase the operating voltage up to 20% if $FeSb_2O_4$ can be used, and this material is also likely to have excellent kinetics even at low temperature. In order to compete with Li-ion batteries, the accessible voltage range must be expanded to >3 V, and intercalation cathodes with higher capacities than La_2CoO_4 or $LaSrMnO_4$ are required.

In summary, we have calculated the properties of different FiB intercalation electrodes, and find that Ca_2N and Y_2C can offer an excellent combination of energy density, power density, and cycling stability. Their useful properties are due to the unique chemistry of layered electrides, which have free anionic electrons occupying vacant anion sites in the defluoridated state. Both materials intercalate F^- with very low kinetic barriers for F^- diffusion, and less volume change than most conversion electrodes, which is ideal for fast and reversible charge/discharge cycles. We expect that these new anodes will significantly advance FiBs' energy storage capability.

AUTHORS' NOTE: During final revision of this manuscript, a new theoretically calculated Ca_2NF phase was added to the Materials Project database. This phase has symmetry *Cm;* while the cation sublattice is the same as the $R\bar{3}m$ phase we identify in this work, the nitride and fluoride anions in the octahedral sites are ordered in a non-layered fashion. The *Cm* phase is calculated to be 26 meV/atom more stable than $R\bar{3}m$, so future work may need to consider if the nitride anions are mobile enough to re-order at battery operating temperatures.

COMPUTATIONAL METHODS

We performed all DFT calculations using the VASP software,[60, 61] and chose our calculation parameters to be compatible with the Materials Project database.[24, 62] Certain calculations could not be converged using the tetrahedron method for electronic smearing, so these were completed using Gaussian smearing with a small SIGMA of 0.01, to minimize the discrepancy compared to the tetrahedron method. To maintain compatibility with the Materials Project, we did not include van der Waals corrections (see Supporting Information for tests of the effects of vdW corrections). All gravimetric capacities were calculated with respect to the mass of the defluoridated or delithiated state, and the reported voltage is the electromotive force driving the complete reaction, which does not include the "steps" seen in many experimental discharge curves due to intermediate phases. The initial locations of fluoride atoms were selected manually,

a procedure which is unambiguous for the layered electrides with their clearly defined octahedral and tetrahedral sites.

We used 3x3x1 supercells for the NEB calculations of Ca_2NF and Y_2CF_2, which contained 81 atoms plus the added fluorine. Ionic positions were relaxed to a force convergence criterion of 0.02 eV/Å, with two exceptions. The Y_2CF_2 interstitial diffusion was terminated after 200 steps because the F^- could not fit through the saddle point, and was taking an alternate route with very high energy. The saddle-point image of Ca_2NF's interstitialcy mechanism was well-converged, but the first image could not be converged even after several hundred ionic steps. The fluorine-poor limit is defined by the Ca_2N/Ca_2NF or Y_2C/Y_2CF_2 equilibrium, while the fluorine-rich limit is the $Ca_2NF/(2CaF_2 + 0.5N_2)$ or $Y_2CF_2/(2YF_3 + C)$ equilibrium.

For the AIMD calculations, we used a slightly larger 120-atom supercell of pristine Y_2CF_2 with no defects, and used only the K-point at gamma to keep the calculations affordable. We used a plane-wave cutoff of 400 eV, a timestep of 2 fs, and kept the cell size and shape fixed. We first heated the cell from 100K to the desired temperature over 2 ps, then allowed 5 ps for the system to reach thermal equilibrium before we began collecting diffusion data. We then calculated the diffusivity as:

$$D = \lim_{t\to\infty}\left[\frac{1}{2dt}\left\langle\left[\vec{r}(t)\right]^2\right\rangle\right] \qquad [5]$$

Where $d = 2$ is the dimension of the diffusion lattice, t is the simulation time, and $\langle[r(t)]^2\rangle$ is the time-averaged mean square displacement (MSD) of the F^- ions.[63] We obtained the activation energy by fitting the temperature-dependent diffusivity data points to an Arrhenius model:

$$D = D_0 \exp\left(-\frac{E_a}{kT}\right) \qquad [6]$$

where D_0 is a constant pre-factor, E_a is the activation energy, k is Boltzmann's constant, and T is the temperature. All AIMD analysis was done using the Mo group aimd post-processing script.[51] Plots of the data are shown in Supporting Information S4.

ASSOCIATED CONTENT

Supporting Information: Performance metrics of other anode materials investigated in this study; effect of van der Waals corrections; decomposition pathways; AIMD data.

AUTHOR INFORMATION

Corresponding author: *Email: S.T.H.(steven.t.hartman@wustl.edu) or R.M.(rmishra@wustl.edu).

Present Address: ⊥(S.T.H.) Materials Science and Technology Division, Los Alamos National Laboratory, Los Alamos, NM 87545, USA.

Conflicts of interest: The authors declare no competing financial interest.

ACKNOWLEDGMENTS

This work was supported by the National Science Foundation (NSF) grant numbers DMREF-1729787 and DMR-1806147. This work used computational resources of the Extreme Science and Engineering Discovery Environment (XSEDE), which is supported by NSF grant number ACI-1548562.

REFERENCES:

1. C. Helbig, A. M. Bradshaw, L. Wietschel, A. Thorenz and A. Tuma, *Journal of Cleaner Production*, 2018, **172**, 274-286.
2. D. H. Doughty and E. P. Roth, *The Electrochemical Society Interface*, 2012, **21**, 37-44.
3. N. Yabuuchi, K. Kubota, M. Dahbi and S. Komaba, *Chemical Reviews*, 2014, **114**, 11636-11682.
4. J. C. Pramudita, D. Sehrawat, D. Goonetilleke and N. Sharma, *Advanced Energy Materials*, 2017, **7**, 1602911.
5. J. Song, E. Sahadeo, M. Noked and S. B. Lee, *The Journal of Physical Chemistry Letters*, 2016, **7**, 1736-1749.
6. D. Kundu, B. D. Adams, V. Duffort, S. H. Vajargah and L. F. Nazar, *Nature Energy*, 2016, **1**, 16119.
7. N. Jayaprakash, S. K. Das and L. A. Archer, *Chemical Communications*, 2011, **47**, 12610-12612.
8. X. Zhao, S. Ren, M. Bruns and M. Fichtner, *Journal of Power Sources*, 2014, **245**, 706-711.
9. X. Zhao, Z. Zhao-Karger, M. Fichtner and X. Shen, *Angewandte Chemie International Edition*, 2019, **0**.
10. M. Oka, H. Kamisaka, T. Fukumura and T. Hasegawa, *Computational Materials Science*, 2019, **167**, 92-99.
11. I. Mohammad, R. Witter, M. Fichtner and M. Anji Reddy, *ACS Applied Energy Materials*, 2018, DOI: 10.1021/acsaem.8b00864.
12. V. K. Davis, C. M. Bates, K. Omichi, B. M. Savoie, N. Momčilović, Q. Xu, W. J. Wolf, M. A. Webb, K. J. Billings, N. H. Chou, S. Alayoglu, R. K. McKenney, I. M. Darolles, N. G. Nair, A. Hightower, D. Rosenberg, M. Ahmed, C. J. Brooks, T. F. Miller, R. H. Grubbs and S. C. Jones, *Science*, 2018, **362**, 1144.
13. M. A. Nowroozi, K. Wissel, J. Rohrer, A. R. Munnangi and O. Clemens, *Chemistry of Materials*, 2017, **29**, 3441-3453.
14. F. Gschwind, G. Rodriguez-Garcia, D. J. S. Sandbeck, A. Gross, M. Weil, M. Fichtner and N. Hörmann, *Journal of Fluorine Chemistry*, 2016, **182**, 76-90.
15. F. Gschwind and J. Bastien, *Journal of Materials Chemistry A*, 2015, **3**, 5628-5634.
16. C. Rongeat, M. Anji Reddy, R. Witter and M. Fichtner, *ACS Applied Materials & Interfaces*, 2014, **6**, 2103-2110.
17. M. Anji Reddy and M. Fichtner, *Journal of Materials Chemistry*, 2011, **21**, 17059-17062.
18. M. A. Nowroozi and O. Clemens, *ACS Applied Energy Materials*, 2018, DOI: 10.1021/acsaem.8b01630.
19. D. T. Thieu, M. H. Fawey, H. Bhatia, T. Diemant, V. S. K. Chakravadhanula, R. J. Behm, C. Kübel and M. Fichtner, *Advanced Functional Materials*, 2017, **27**, 1701051.
20. L. Zhang, M. A. Reddy and M. Fichtner, *Journal of Solid State Electrochemistry*, 2018, **22**, 997-1006.
21. A. Kraytsberg and Y. Ein-Eli, *Journal of Solid State Electrochemistry*, 2017, **21**, 1907-1923.
22. M. A. Nowroozi, S. Ivlev, J. Rohrer and O. Clemens, *Journal of Materials Chemistry A*, 2018, **6**, 4658-4669.
23. K. Lee, S. W. Kim, Y. Toda, S. Matsuishi and H. Hosono, *Nature*, 2013, **494**, 336-340.
24. A. Jain, S. P. Ong, G. Hautier, W. Chen, W. D. Richards, S. Dacek, S. Cholia, D. Gunter, D. Skinner, G. Ceder and K. A. Persson, *APL Materials*, 2013, **1**, 011002.
25. A. K. Padhi, K. S. Nanjundaswamy and J. B. Goodenough, *Journal of The Electrochemical Society*, 1997, **144**, 1188-1194.
26. K. Mizushima, P. C. Jones, P. J. Wiseman and J. B. Goodenough, *Materials Research Bulletin*, 1980, **15**, 783-789.
27. R. Shannon, *Acta Crystallographica Section A*, 1976, **32**, 751-767.

28. S. V. Krivovichev, O. Mentré, O. I. Siidra, M. Colmont and S. K. Filatov, *Chemical Reviews*, 2013, **113**, 6459-6535.
29. M. Naguib, V. N. Mochalin, M. W. Barsoum and Y. Gogotsi, *Advanced Materials*, 2014, **26**, 992-1005.
30. M. A. Nowroozi, B. de Laune and O. Clemens, *ChemistryOpen*, 2018, **7**, 617-623.
31. W. Zaheer, J. L. Andrews, A. Parija, F. P. Hyler, C. Jaye, C. Weiland, Y.-S. Yu, D. A. Shapiro, D. A. Fischer, J. Guo, J. M. Velázquez and S. Banerjee, *ACS Energy Letters*, 2020, **5**, 2520-2526.
32. K. Wissel, S. Dasgupta, A. Benes, R. Schoch, M. Bauer, R. Witte, A. D. Fortes, E. Erdem, J. Rohrer and O. Clemens, *Journal of Materials Chemistry A*, 2018, DOI: 10.1039/C8TA01012A.
33. A. Simon, *Coordination Chemistry Reviews*, 1997, **163**, 253-270.
34. K. Omichi, Q. Xu and C. Brooks, https://patents.google.com/patent/US20190103607A1/en, 2019.
35. C. Hadenfeldt and H. Herdejürgen, *Zeitschrift für anorganische und allgemeine Chemie*, 1987, **545**, 177-183.
36. A. Bowman, P. V. Mason and D. H. Gregory, *Chemical Communications*, 2001, DOI: 10.1039/B105448C, 1650-1651.
37. R. A. Nicklow, T. R. Wagner and C. C. Raymond, *Journal of Solid State Chemistry*, 2001, **160**, 134-138.
38. K. Wissel, J. Heldt, P. B. Groszewicz, S. Dasgupta, H. Breitzke, M. Donzelli, A. I. Waidha, A. D. Fortes, J. Rohrer, P. R. Slater, G. Buntkowsky and O. Clemens, *Inorg. Chem.*, 2018, DOI: 10.1021/acs.inorgchem.8b00661.
39. O. Clemens and R. Slater Peter, *Journal*, 2013, **33**, 105.
40. M. Holland, N. Charles, J. M. Rondinelli and K. R. Poeppelmeier, *J. Am. Chem. Soc.*, 2016, **138**, 11882-11889.
41. E. T. Keve and A. C. Skapski, *Chemical Communications (London)*, 1966, DOI: 10.1039/C19660000829, 829-830.
42. W. Sun, S. T. Dacek, S. P. Ong, G. Hautier, A. Jain, W. D. Richards, A. C. Gamst, K. A. Persson and G. Ceder, *Science Advances*, 2016, **2**.
43. M. Atoji and M. Kikuchi, *The Journal of Chemical Physics*, 1969, **51**, 3863-3872.
44. D. L. Druffel, M. G. Lanetti, J. D. Sundberg, J. T. Pawlik, M. S. Stark, C. L. Donley, L. M. McRae, K. M. Scott and S. C. Warren, *Chemistry of Materials*, 2019, DOI: 10.1021/acs.chemmater.9b03722.
45. A. Urban, D.-H. Seo and G. Ceder, *npj Computational Materials*, 2016, **2**, 16002.
46. K. Momma and F. Izumi, *J. Appl. Crystallogr.*, 2011, **44**, 1272-1276.
47. G. Henkelman, B. P. Uberuaga and H. Jónsson, *The Journal of Chemical Physics*, 2000, **113**, 9901-9904.
48. M. Okubo, Y. Tanaka, H. Zhou, T. Kudo and I. Honma, *The Journal of Physical Chemistry B*, 2009, **113**, 2840-2847.
49. K.-T. Vassiliki and S. Efthimios, *Open Physics*, 2010, **8**, 900-904.
50. K. Schmalzl, *Physical Review B*, 2007, **75**, 014306.
51. X. He, Y. Zhu, A. Epstein and Y. Mo, *npj Computational Materials*, 2018, **4**, 18.
52. X. He, Y. Zhu and Y. Mo, *Nature Communications*, 2017, **8**, 15893.
53. L. N. Patro and K. Hariharan, *Solid State Ionics*, 2013, **239**, 41-49.
54. Q. Zhu, T. Frolov and K. Choudhary, *Matter*, 2019, DOI: https://doi.org/10.1016/j.matt.2019.06.017.
55. L. A. Burton, F. Ricci, W. Chen, G.-M. Rignanese and G. Hautier, *Chemistry of Materials*, 2018, **30**, 7521-7526.
56. T. Tada, S. Takemoto, S. Matsuishi and H. Hosono, *Inorganic Chemistry*, 2014, **53**, 10347-10358.
57. M. M. Menamparambath, J.-H. Park, H.-S. Yoo, S. P. Patole, J.-B. Yoo, S. W. Kim and S. Baik, *Nanoscale*, 2014, **6**, 8844-8851.

58. P. A. Anderson, *Physical Review*, 1949, **75**, 1205-1207.
59. A. Grenier, A. G. Porras-Gutierrez, M. Body, C. Legein, F. Chrétien, E. Raymundo-Piñero, M. Dollé, H. Groult and D. Dambournet, *The Journal of Physical Chemistry C*, 2017, **121**, 24962-24970.
60. G. Kresse and D. Joubert, *Physical Review B*, 1999, **59**, 1758-1775.
61. G. Kresse and J. Furthmüller, *Physical Review B*, 1996, **54**, 11169-11186.
62. S. P. Ong, W. D. Richards, A. Jain, G. Hautier, M. Kocher, S. Cholia, D. Gunter, V. L. Chevrier, K. A. Persson and G. Ceder, *Computational Materials Science*, 2013, **68**, 314-319.
63. Y. Mo, S. P. Ong and G. Ceder, *Chemistry of Materials*, 2012, **24**, 15-17.